2010 IEEE International Conference on Robotics and Automation
Anchorage Convention District
May 3-8, 2010, Anchorage, Alaska, USA

Three-Dimensional Human Arm and Hand Dynamics and Variability Model for a Stylus-based Haptic Interface

Michael J. Fu, and M. Cenk Çavuşoğlu

Abstract— **Human-computer/machine interface research benefits from accurate human arm models for stability analysis, control, and system design. The current study developed models for human arm dynamics and variability specific to stylus-based kinesthetic haptic interfaces. Data from nine human subjects (5 male, 4 female, ages 20–30) were collected using a three degree-of-freedom haptic device in the X, Y, and Z axes along with a range of grip forces (1–3N) for parametric system identification of the human arm and hand. Variability models that accounted for subject and grip force variation were also identified. The arm and hand model structure consisted of a third-order linear parametric transfer function that was paired with a previously derived second-order model for the haptic robot. The variability was modeled as multiplicative unstructured uncertainty using transfer functions. All of the model parameters were identified in the frequency domain and have force as input and position as output.**

I. INTRODUCTION

Kinesthetic haptic interfaces provide a human operator bilateral force interaction with a remote or virtual environment. The human arm, with its amazing sensing ability, countless configurations, and multitude of applications is by far the most complex and variable element in any haptic interface system. In order to develop a stable and useful haptic interface, accurate and relevant models of human arm dynamics are a necessity. They are critical for proper stability analysis, interface design, and improving haptic fidelity. However, because the human arm is so dextrous and reconfigurable, researchers have reported that small variations in arm configurations, grip forces, and application environments result in the arm exhibiting a wide range of dynamic behavior [1]–[4]. Therefore, arm orientations relevant to a task should be considered during model identification. The current study focuses on modeling the arm and hand for stylus-handled haptic interfaces. Stylus handles are commonly found on commercially available haptic interfaces and are convenient for mimicking tools such as paintbrushes, dentistry instruments, and surgical blades.

The models developed in this study used the common convention of force at the hand as the model input and measured hand position as model output. This formulation was consistent with the impedance model for human interaction and the two-port framework for haptic interfaces [5], [6]. Also, since human subjects exhibit significant variations in their performance, the current work developed models for maximum inter and intra-subject variability that are valuable for robust stability analysis of haptic interface systems.

Dynamic models for the human arm originated with researchers investigating the body's biomechanics [7]–[10]. As robotics and haptic technology became more mature, researchers began to develop single-input-single-output models based on mass-spring-dampers systems, which have been shown to accurately reflect arm dynamics and are more suitable for real-time computer implementation [10]–[13]. More recently, human arm dynamics have been modeled using haptic interfaces in an effort to improve system design and fidelity. Hasser developed a grasping model while operating a haptic knob [14]. Woo and Lee characterized the inertia, stiffness, and viscosity of the arm exerting forces of 0–20 N using a one degree-of-freedom (1 DOF) robot [15]. Dong et al. described non-parametric frequency responses of human fingers using various grip configurations subjected to a random vibration [16]. Kuchenbecker et al. used a stylus handle with a grip force sensor on a 1 DOF manipulator to characterize the hand and wrist [2]. Vlugt and Schouten modeled intrinsic and reflexive muscle parameters for the shoulder, elbow, and wrist joints using a 2D planar robot [17]. Speich et al. characterized human arm parameters using a 3 DOF robot with a stylus handle [18].

The mentioned works contributed greatly to haptics research, but what is missing from the literature are experimentally-derived models describing the variation found in human arm dynamics. Studies have modeled the variation as arbitrarily-selected non-linear impedances and as unstructured/structured uncertainty, but these were derived without human experiment [19], [20]. Others reported the amount of variance observed in data collections and parameter identifications, but the variances are not modeled in a way that can be directly used for robust stability analysis. The current work modeled the inter and intra-subject variability due to grip force changes and human variation.

Also, the accuracy of existing arm dynamics models can be improved upon by including the haptic device's dynamics in the model structure, which has not been done. Accurate models for haptic robots exist, so they should be and are included in the current work's model structures to account for their effects on experimental data.

Study Objectives

This study used data collected from human experiments to identify a 3D Cartesian-space model of the human arm and

This work was supported in part by NSF grant CNS-0423253, IIS-0805495, and US DoC under grant TOP-39-60-04003.

M. J. Fu is with the Department of Electrical Engineering and Computer Science, Case Western Reserve University, Cleveland, OH 44106, USA mjfu@case.edu

M. C. Çavuşoğlu is with the Faculty of the Department of Electrical Engineering and Computer Science, Case Western Reserve University, Cleveland, OH 44106, USA cavusoglu@case.edu

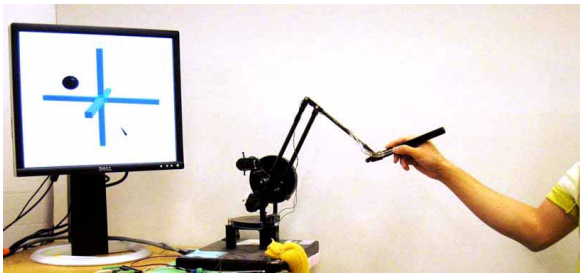

Fig. 1. The experimental setup and arm configuration used for the human experiment data collections.

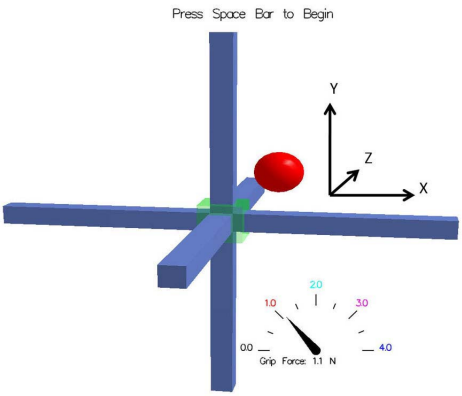

Fig. 2. Computer interface seen by the subjects. The blue cross bars give the user a fixed coordinate frame to judge 3D motion by. The sphere is the cursor controlled by the stylus, which changes color to correspond to the label used for each grip force in the gauge (lower right of the screen). The green transparent box at the center of the crossbars was the static position subjects were instructed to maintain during the experiment.

subject variation using force as the model input and position as output. The arm was modeled using five-parameter linear transfer functions based on the dynamics of one mass, two springs, and two dampers. Variances were modeled as multiplicative unstructured uncertainty using transfer functions with up to five stable complex-conjugate pairs of poles and five minimum-phase complex-conjugate pairs of zeros.

II. Methods

A. Subjects

Nine right hand dominant subjects (4 female, 5 male, ages 20–30) were recruited with prior consent for this study and were not compensated for their participation. Each subject was free from movement impairments relevant to this study and tested using their right arm. The experiment procedures were reviewed and given exemption status by the institution's Internal Review Board.

B. Equipment

Experiments were performed using a PHANToM Premium 1.5a haptic interface (Sensable Technologies Corp., Woburn, MA) equipped with a FlexiForce force-sensitive resistor to sense grip forces (TekScan Corp., Boston, MA). A Phidgets Inc. (Calgary, Alberta, Canada) 1018 analog-to-digital interface was used to acquire data from the grip force sensor at 65 Hz. A dual-core 2.53 GHz Xenon workstation (Dell Corp, Round Rock, TX) ran a real-time servo loop of 1 kHz and acquired data using a PCI-6602 counter (National Instruments Corp., Austin, TX). Output to the motor amplifiers was performed using a PCI-DDA08/12 digital-to-analog converter (Measurement Computing Corp., Norton, MA).

C. System Identification with Human Subjects

Performing system identification using input signals such as frequency sweeps, discrete sinusoidal signals, and random noise typically produce comparable results [21]. However, when modeling the human arm, frequency sweeps and discrete sine waves are not suitable because at low frequencies (< 3 Hz), human reflexes make it difficult to keep the arm passive to force disturbances. Fortunately, the more random the force disturbance is, the less likely it will trigger the arm's reflexes. For this reason, the current study used Gaussian white noise inputs with a bandwidth of 30 Hz to render the input forces unpredictable by human subjects.

The gaussian white noise was low-pass filtered to 30 Hz because of the limits imposed by neural signal delay for voluntary movement. During complex tasks, such as target reaching, humans take up to 110 ms to respond to changes in target position [22]. It takes approximately 75 ms for a neural signal to travel from the brain to the ankle muscles and back [23]. For the wrist, Marsden et al. found that it takes approximately 50 ms to resist an extension by an external force [24]. Since the arm is closer to the brain than the ankle and the target in this study is static, 50 ms was assumed as the approximate time delay for the arm in the experimental task. Under this assumption, the bandwidth for the human arm was approximated to 20 Hz, justifying the selection of 30 Hz noise bandwidth.

D. Arm Model Experiment Paradigm

During the experiments, hand position data in all 3 degrees of movement (X being left and right, Y being up and down, and Z being forward and backward) were recorded while the subject's arm was stimulated with random forces in only one of the degrees of movement. The duration of stimulation lasted 50–100 s depending on the ability the subject to maintain a consistent grip force. A consistent grip force was defined to be within ± 0.5 N of the desired force and verified visually by the experimenter. In order not to exceed the 3 A current limit on the PHANToM's motors, the forces at the stylus were limited to ≤ 5 N. Nine sets of data were collected from each subject, one for every combination of three grip forces (1, 2, and 3 N) and three directions of force stimulation (X, Y, and Z directions). The grip forces were selected because grip forces less than 1 N were insufficient for holding onto the stylus under the stimulation forces and forces greater than 3 N were very difficult to hold for longer than 100 s.

For each test, the subject was instructed to sit facing a 19" computer monitor in a chair with no arm rests and to use their hand to hold a stylus-shaped handle attached to the

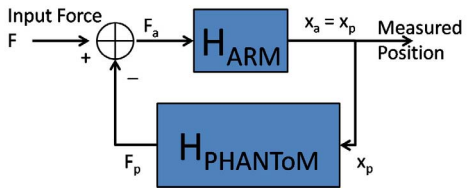

Fig. 3. Block diagram of the human arm coupled to the PHANToM haptic device. H_{ARM} represents the lumped model of the arm's passive and controlled dynamics and $H_{PHANToM}$ represents the position-input/force-output dynamics of the PHANToM haptic interface as presented in [25]. Input force F represents the motor forces, F_a the force input to H_{ARM}, and F_p the force output of $H_{PHANToM}$. Position $x_a = x_p$ represents the hand and stylus positions, respectively.

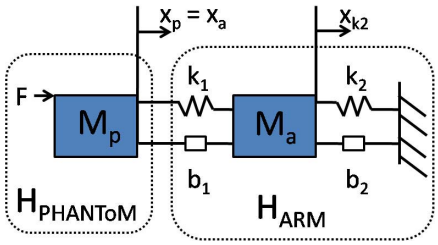

Fig. 4. Free-body diagram of the arm and the PHANToM. The dashed box on the left corresponds to the $H_{PHANToM}$ block in Fig. 3 and the components in the dashed box on the right correspond to the H_{ARM} block. Mass M_p is the inertia of the PHANToM and mass M_a the inertia of the arm. Elements k_1 and k_2 are springs, while b_1 and b_2 are dampers. External force F is from the PHANToM's motors. Position x_p is the position of the stylus handle, which is euqal to the position of the hand, x_a

end-effector of the PHANToM robot as one grasps a pen. Figure 1 shows the arm configuration and experiment setup. Figure 2 shows the graphic user interface (GUI) presented to the subject. The GUI displays a spheroid cursor that reflects the motion of the stylus tip on a 1:1 scale in virtual 3D space. The subject's grip force was displayed in two ways: using a gauge and by changing the color of the sphere to signal that a certain grip force was achieved (red for 1 N, cyan for 2 N, and magenta for 3 N). The color changes prevent the subject from diverting their attention from the cursor to the force gauge.

Using the GUI and the PHANToM stylus, the subject was instructed to maintain one of the three tested grip forces throughout the duration of the trial and attempt to keep the cursor at the static target in the center of the crossbars (transparent green box in Fig. 2). Once the subject achieved the desired grip force and centered the cursor within the box, they initiated stimulation forces by pressing a button with their untested hand. Once each trial was over, the subject was given as much time as needed to rest. The experimenter visually verified that grip forces did not exceed a tolerance of $\pm$0.5 N and that the cursor position did not drift away from the center target. Once the subject was ready again, another random combination of grip force and stimulation direction was tested.

E. Arm Model Structure

The model structure in Fig. 3, referred to from here on as the 'measured-dynamics model', was a feedback loop between the PHANToM haptic interface and a lumped model of the arm's passive and active control dynamics. In both Figs. 3 and 4, force F represents the PHANToM's motor forces, which are those used for system identification. Forces F_a and F_p in Fig. 4 are not external forces, but are the force input to H_{ARM} (referred to as the 'arm dynamics' from here on) and force output to $H_{PHANToM}$, respectively. Positions $x_a = x_p$ are the measured hand and stylus handle positions, which were assumed to be equal. The PHANToM's dynamics were the transfer function models described by Cavusoglu et al. [25]. Although Cavusoglu's models were identified at the motors, the current study applied them to the end effector of the haptic device by assuming that the links are rigid for frequencies $\leq$ 30 Hz.

A transfer function for the arm dynamics model structure was constructed from Fig. 4. The free-body diagram (Fig. 4) and the block diagram (Fig. 3) are equivalent by the definitions

$$F_a = F - F_p \tag{1}$$

where F is the force exerted by the PHANToM motors and

$$F_a = -\big(k_1(x_{k2} - x_p) + b_1(\dot{x}_{k2} - \dot{x}_p)\big),$$

Conveniently, all three of the PHANToM's degrees of freedom behave as a simple mass for the frequency bandwidth of interest in this study ($\leq$ 30 Hz). Thus, for system identification purposes, the PHANToM's transfer function for all 3 DOFs was modeled as

$$H_{PHANToM}(s) = \frac{F_p(s)}{X_p(s)} = M_p s^2,$$

where $F_p(s) = F(s) - F_a(s)$, as defined in (1), $X_p(s)$ was the frequency spectrum of the measured stylus tip position, and M_p was the same as in Fig. 4 approximated about the operating point as

$$\begin{aligned} M_p^x &= 0.09kg \\ M_p^y &= 0.095kg \\ M_p^z &= 0.091kg. \end{aligned} \tag{2}$$

The arm dynamics model transfer function was derived from the 5 parameters M_a, k_1, k_2, b_1, and b_2 in Fig. 4 in Laplace notation as

$$H_{ARM}(s) = \frac{X_a(s)}{F_a(s)} = \frac{M_a s^2 + (b_1+b_2)s + k_1 + k_2}{b_1 M_a s^3 + (b_1 b_2 + k_1 M_a)s^2 + (b_2 k_1 + b_1 k_2)s + k_1 k_2}, \tag{3}$$

where $X_a(s)$ was the frequency spectrum of the hand position and $F_a(s) = F(s) - F_p(s)$, from (1). The closed-loop combination of the arm and PHANToM models was the measured-dynamics model

$$H_{CL}(s) = \frac{Position}{Force} = \frac{H_{ARM}(s)}{1 + H_{ARM}(s)H_{PHANToM}(s)}, \tag{4}$$

which resulted in a fourth-order transfer function that was fitted to the human experiment data to identify M_a, k_1, k_2, b_1, and b_2. Each fit was performed using nonlinear constrained optimization (Matlab `fmincon.m` function) in the frequency domain by minimizing the cost function

$$\sum_{n=1}^{k=3000} W_t(n)\left[20log_{10}\big(H_{exp}(j2\pi\frac{n}{N}) - H_{CL}(j2\pi\frac{n}{N})\big)^2\right], \quad (5)$$

where $W_t(n)$ was a weighting function used to fine-tune the fit at each data sample, $H_{exp}(j\omega)$ was the frequency response of the human experiment data, $H_{CL}(j\omega)$ was the measured-dynamics model's frequency response from (4), $k = 3000$ was the number of data samples for 30 Hz of data, and N was 10^5, the number of samples from 100 s of data acquired at 1 kHz. $H_{exp}(j\omega)$ was calculated from the 81 total measured-dynamics frequency responses (9 subjects, 3 axes, 3 grip forces) as described in the next two sections. Each individual measured-dynamics frequency response was computed by taking the FFT of the measured time-domain position output data and dividing it by the FFT of the generated time-domain white noise force input signal, both windowed by 100dB sidelobe Chebyschev windows (using Matlab's `fft.m` and `chebwin.m` functions).

Equation (5) was used as the cost function to identify two sets of arm dynamics model parameters M_a, k_1, k_2, b_1, and b_2, as follows:

1) Set 1: Grip-Force-Dependent Arm Model Parameters: Parameters for the first set were derived from nine measured-dynamics model fits, one for each grip force at each axis. In each model, $H_{exp}(j\omega)$ from (5) was defined as the 81 measured-dynamics frequency response averaged over all subjects, resulting in nine grip-force-dependent arm models. These models are presented in Sec. III-A.

2) Set 2: Nominal Arm Model Parameters: Parameters in the second set were identified from three measured-dynamics model fits, one for each axis. The fits were obtained by defining $H_{exp}(j\omega)$ from (5) as the median of the 81 measured-dynamics frequency responses over all subjects and all grip forces. Then, the identified parameters were used to compute the nominal arm model transfer function, referred to from here on as $\hat{H}_{ARM}(s)$, using (3). These models do not include the PHANToM dynamics, are reported in Sec. III-B, and were used as the nominal models to calculate unstructured uncertainty in the following section.

F. Variability Model Structure

Consistent with robust control theory, the variability of the system was considered to be unstructured multiplicative uncertainty [26]. In this formulation, the uncertainty model is defined as follows:

For a system with plant transfer function $P(j\omega)$,

$$P(j\omega) \in \{\hat{P}(j\omega)\big(1 + W_u(j\omega)\Delta(j\omega)\big) : sup|\Delta(j\omega)| \le 1\},$$
$$\Delta \in \mathcal{R}$$

where $\hat{P}(j\omega)$ is the nominal plant transfer function, $W_u(j\omega)$ is the uncertainty weighting function, and $\mathcal{R}$ is the set of proper real rational functions. The uncertainty weighting function $W_u(j\omega)$ has the relationship

$$|W_u(j\omega)| \ge \left|\frac{P(j\omega)}{\hat{P}(j\omega)} - 1\right| \quad (6)$$

and can be interpreted as the percentage uncertainty relative to the nominal plant $\hat{P}(j\omega)$ at frequency ω.

In this study, the haptic device dynamics were assumed to have no uncertainty, so $W_u(j\omega)$ represented the variability of the experimental arm dynamics (excluding the PHANToM dynamics) with respect to the nominal arm model described in Sec. II-E.2. In order to satisfy (6), $W_u(j\omega)$ was selected to be the maximum of the right side of (6) at each frequency with $P(j\omega)$ defined as the derived-arm-dynamics, refered to as $H^{exp}_{ARM}(s)$, and $\hat{P}(j\omega)$ defined as the nominal arm transfer functions $\hat{H}_{ARM}(s)$. Consistent with Fig. 3, the derived-arm-dynamics

$$H^{exp}_{ARM}(s) = \frac{X_a(s)}{F_a(s)}$$

were computed using Welch's transfer function estimation (Matlab's `tfestimate.m`, with four Hamming windowed segments and 50% overlap) with time-domain measured arm position, $x_a(t)$ as the transfer function input and time-domain force $F_a(t)$ as the output. $F_a(t)$ was derived by removing the PHANToM dynamics from the measured experimental frequency response using the relationship

$$F_a(t) = F(t) - F_p(t),$$

from (1). $F(t)$ was the generated white noise system identification input forces and $F_p(t)$ was approximated by the second derivative of the measured hand position, $x_a(t)$, as

$$F_p(t) = M_p\big(\frac{d^2x_a(t)}{dt^2}\big),$$

with M_p as defined in (2) and the second derivative approximated by

$$\frac{d^2x[n]}{dt^2} = \frac{x_a[n+1] - 2x_a[n] + x_a[n-1]}{\Delta t^2}$$

with Δt as 0.001 s.

For each axis, the uncertainty was modeled by a stable and minimum-phase transfer function of the form

$$\hat{W}_u(s) = K\frac{\prod_{i=1}^{N_n}(s - z_i)}{\prod_{i=1}^{N_d}(s - p_i)} \quad (7)$$

with a scaling term K, stable poles p_i, numerator order N_n, minimum-phase zeroes z_i, and denominator order N_d. This model was fitted to envelope the maximum uncertainty observed in all subjects and all grip forces using the Matlab's `fmincon.m` function. Each transfer function was constrained to have $N_n \ge N_d$ so that the modeled uncertainty would not asymptotically approach zero. The cost function used was

$$\sum_{n=1}^{k=3000} W_t(n)\left[20log_{10}\big(\hat{W}_u(j2\pi\frac{n}{N}) - W_u^{max}(j2\pi\frac{n}{N})\big)^2\right],$$

TABLE I

ARM MODEL PARAMETERS FROM SYSTEM IDENTIFICATION

X-axis	M_a (kg)	k_1 (N/m)	k_2 (N/m)	b_1 (N·s/m)	b_2 (N·s/m)
1N grip	0.1925	85.48	704.2	7.410	2.477
2N grip	0.2037	76.29	785.4	7.598	2.532
3N grip	0.2057	88.91	784.3	7.592	2.525
Y-axis	M_a (kg)	k_1 (N/m)	k_2 (N/m)	b_1 (N·s/m)	b_2 (N·s/m)
1N grip	0.2775	91.48	649.4	7.217	4.314
2N grip	0.2984	84.85	779.8	7.632	4.919
3N grip	0.2954	86.84	775.1	7.719	4.541
Z-axis	M_a (kg)	k_1 (N/m)	k_2 (N/m)	b_1 (N·s/m)	b_2 (N·s/m)
1N grip	4.374	4877	200.4	55.85	32.96
2N grip	2.250	2196	181.1	40.83	30.56
3N grip	3.107	3289	120.8	50.16	29.70

TABLE II

NOMINAL ARM MODEL PARAMETERS

Axis	M_a (kg)	k_1 (N/m)	k_2 (N/m)	b_1 (N·s/m)	b_2 (N·s/m)
X-axis	0.2277	59.39	628.0	5.514	9.161
Y-axis	0.4142	98.27	421.2	5.720	9.766
Z-axis	1.628	564.7	130.6	37.14	35.36

TABLE III

UNCERTAINTY WEIGHTING FUNCTION POLES AND ZEROES

	X-axis	Y-axis	Z-axis
K	1.2252	0.6247	1.7911
Zeros 1	$-1.859 \pm 2.731j$	$-1.798 \pm 4.368j$	$-25.89 \pm 69.80j$
Zeros 2	$-8.135 \pm 13.27j$	$-7.786 \pm 43.84j$	$-6.240 \pm 19.61j$
Zeros 3	$-38.59 \pm 21.41j$	$-22.03 \pm 137.2j$	$-12.02 \pm 56.21j$
Zeros 4	$-2.862 \pm 47.72j$	$-239.3 \pm 67.64j$	–
Zeros 5	$-35.79 \pm 6.553j$	$-11.05 \pm 29.71j$	–
Poles 1	$-4.082 \pm 48.37j$	$-26.36 \pm 133.6j$	$-6.505 \pm 19.85j$
Poles 2	$-5.473 \pm 12.19j$	$-144.8 \pm 25.81j$	$-11.30 \pm 62.12j$
Poles 3	$-15.08 \pm 34.74j$	$-8.834 \pm 38.78j$	$-31.10 \pm 74.87j$
Poles 4	$-1.535 \pm 1.709j$	$-2.796 \pm 3.038j$	–
Poles 5	$-69.14 \pm 3.793j$	$-28.95 \pm 38.84j$	–

where $W_t(n)$ was a weighting function, $\hat{W}_u(j\omega)$ was the transfer function model in (7), $W_u^{max}(j\omega)$ was the maximum value of the right side of (6) at each frequency across all subjects and grip forces, $k = 3000$ was the number of data samples for 30 Hz of data, and N was 10^5, the number of samples from 100 s of data accquired at 1 kHz.

III. RESULTS

A. Grip-Force-Dependent Measured-Dynamics Models Results

Nine measured-dynamics models were identified in total, each with force as input and position as output. For each of the three tested grip forces, an X-output/X-input, Y-output/Y-input, and Z-output/Z-input model was identified. All the fitted parameters are in Table I and Bode plots of the models are shown in Fig. 5.

Each model was identified to accurately reflect the experimental data across 0.1–30 Hz and also capture the resonant peaks observed at approximately 15 Hz for the X and Y axes and 5 Hz for the Z-axis.

B. Variance Model Results

A total of three unstructured uncertainty variance models were identified, one for each of the X, Y, and Z axes. The

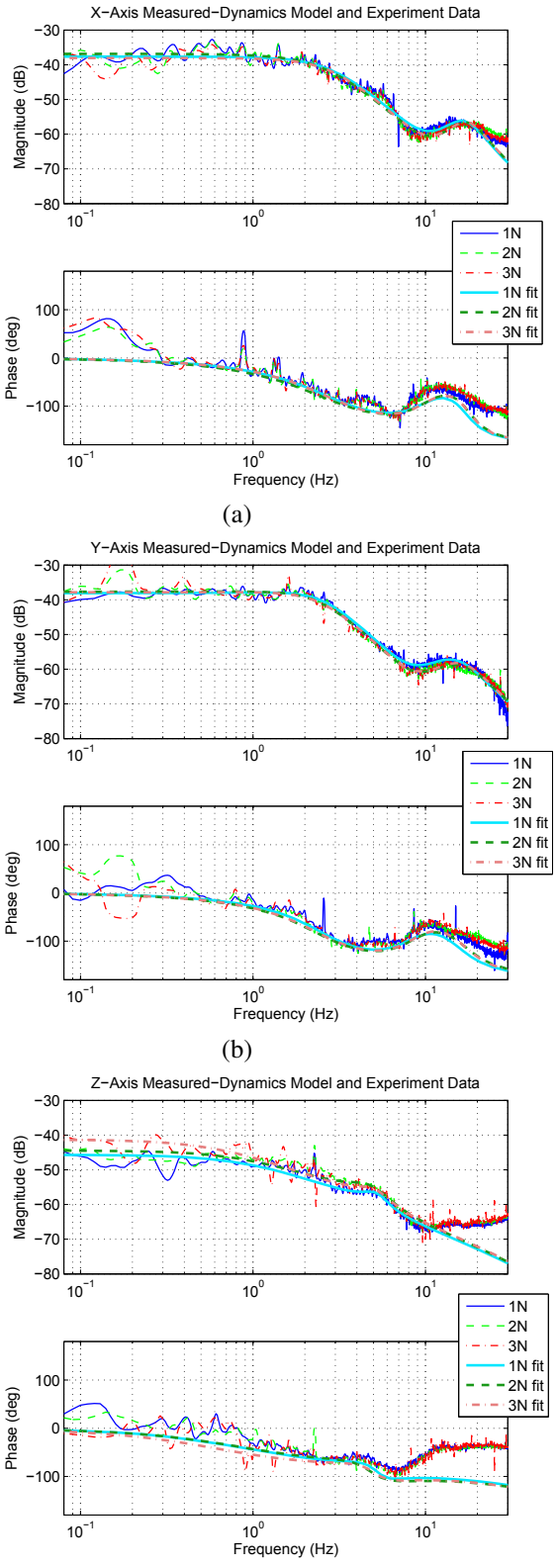

Fig. 5. (a)–(c) The thicker lines are the frequency responses of the grip-force dependent X, Y, and Z-axis measured-dynamics models, which include the PHANToM dynamics. The thinner lines are the frequency response of the experimental measured-dynamics. The model parameters are in Table I.

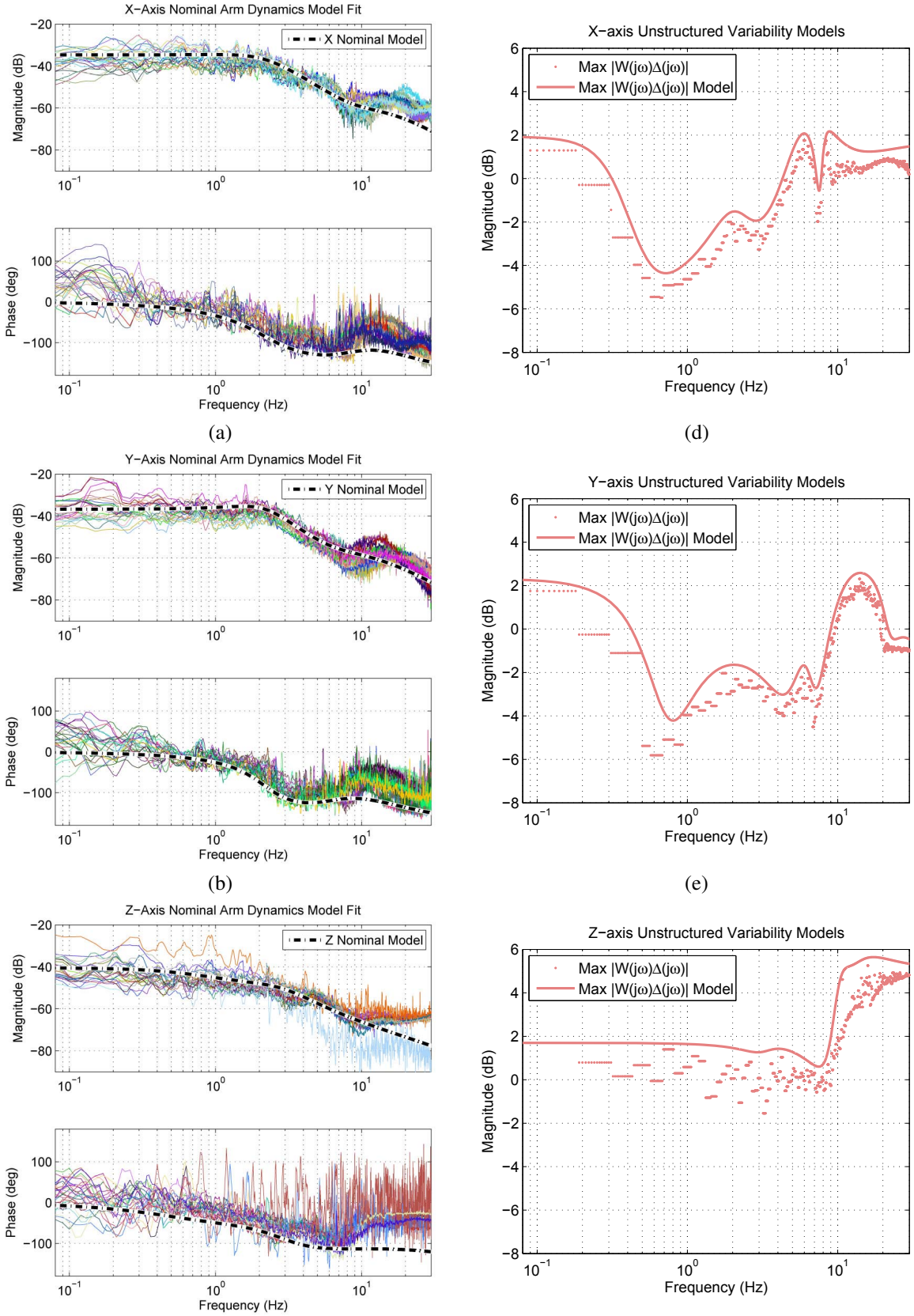

Fig. 6. (a)–(c) For each axis, black dash-dot lines are the frequency response of the nominal arm models, $\hat{H}_{ARM}(s)$ as described in Sec. II-E.2. The multiple thin lines show the 81 derived-arm-dynamics frequency responses described in Sec. II-F. The parameters of the nominal arm models are given in Table II. The nominal arm models were used in (6). (d)–(f) Magnitude response for the inter/intra-subject unstructured uncertainty weighting functions of the X, Y, and Z axes (solid lines) are plotted along with the maximum uncertainty they were modeled after (dots).

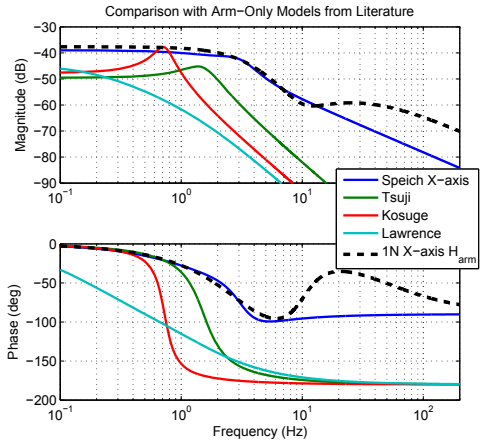

Fig. 7. The frequency responses of different models reported in literature (solid color lines) plotted along with the current study's 1N X-axis $H_{ARM}(s)$ model (black dashed line).

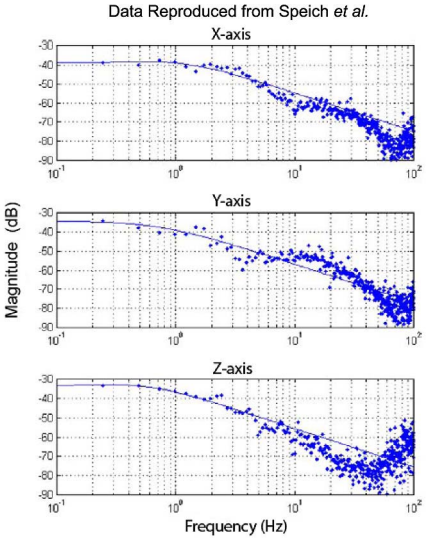

Fig. 8. Speich et al.'s model magnitude response (solid lines) plotted over experimental data (dots). Reprinted with permission from [18].

variance models captured the maximum uncertainty observed in all of the nine subjects and 1–3N grip forces for 0.01–30 Hz. The fit parameters are listed in Table III. Each variance model was a transfer function consisting of up to five stable complex-conjugate pole pairs and five minimum-phase zero pairs. Figure 5.d–f shows the frequency response of each variance model (solid lines) enveloping the maximum experimental uncertainty (dotted lines).

Also, in order to calculate the unstructured uncertainty, three nominal arm-dynamics models were identified. The nominal model parameters are listed in Table II and their frequency responses are plotted in Fig. 6.a–c (thick dot-dashed lines) along with the 81 individual derived-arm-dynamics frequency responses of each subject (thin solid lines).

IV. Discussion

The proposed measured-dynamics model structure accurately matched the overall frequency response of the experimental data between 0.1–30 Hz for the X and Y axes and 0.1–10 Hz for the Z-axis. The Z-axis was not fitted to the experimental data between 10-30 Hz because in that frequency range, the measured magnitude response rose at a rate of approximately 15 dB/dec. This gives rise to the possibility for a resonant peak existing beyond 30 Hz, which may be the result of coupling effects between the Y and Z axes caused by the kinematics of the arm during the Z-axis stimulation. Specifically, The elbow joint was observed to stiffen when the subject maintains a grip force and tries to stabilize the stylus. However, since the force input bandwidth was limited to 30 Hz, further study is required in order to determine how to best model the z-axis frequency response past 10 Hz. Therefore, the Z-axis model's frequency response was designed to be dominated by the M_a mass parameter at frequencies past 10 Hz, which is why the model's frequency response falls off at 40 dB/dec between 10–30 Hz (Fig. 5.c).

The identified models also captured local minima in the magnitude response observed for the X and Y axes centered around 10 Hz (Fig. 5.a–c). Similar local minima in the arm's experimental magnitude response were found in Speich et al.'s study, which also modeled the human arm using a 3 DOF stylus-based manipulator [18]. Speich's results (Fig. 8) show the local minima for the experimental magnitude response (blue dots) centered around 10 Hz for the X-axis and 4 Hz for the Y-axis.

However, the models proposed by Speich et al. [18], Kosuge et al. [13], Lawrence [12], and Tsuji et al. [10] did not exhibit this resonant depression behavior. Speich et al. used a five-parameter model (similar to the current work, but without including the haptic device dynamics), which can be expressed as in (3). Tsuji, Kosuge, and Lawrence used 3-parameter models (mass m, spring k, damper b) resulting in a second-order transfer function expressed by

$$\frac{position}{force} = \frac{1}{ms^2 + bs + k}.$$

Figure 7.a shows that the current models' frequency responses were within the range of previous studies and exhibit high-frequency dynamics absent from existing models. The plotted 1N X-axis $H_{arm}(s)$ dynamics were computed by (3) using parameters from Table I. Speich et al.'s model has a relative order of 1, so the drop off is 20 dB/dec after about 3 Hz. The other three models in Fig. 7 are all second order, droping off at 40 dB/dec even earlier, from 1–2 Hz. The current model, however, maintains valuable dynamics that occur past 10 Hz and then falls off at 40 dB/dec. This was consistent with both the experimental data and the expectation for the arm to behave like a mass at frequencies beyond those relevant to voluntary control, which should behave as a second order system falling off at 40 dB/dec.

It was also observed that the identified parameters of the current model structure were in the range of existing results. As reported in Table I, the mass parameters of the

TABLE IV
ARM MODEL PARAMETERS FROM LITERATURE

	M_a(kg)	k_1(N/m)	k_2(N/m)	b_1(N·s/m)	b_2 (N·s/m)
Speich X	0.85	122	330	12.9	12.9
Speich Y	4.03	108	104	9.20	47.6
Speich Z	0.68	81.4	13.0	17.6	13.5
Speich 1DOF	1.46	48.8	375	4.5	7.9
Kosuge	11.6	243	–	17	–
Lawrence	17.5	175	–	175	–
Tsuji	3.25	300	–	20	–

current models were identified to be between 0.19–4.37 kg, which overlaped the range of 0.68–17.5 kg reported by previous studies (Table IV). This study's identified stiffness parameters ranged from 76–4877 N/m for k_1 and 120–785 N/m for k_2, which overlaps and slightly exceeds the range of 48.8–300 N/m reported in literature. The current results also showed that damping parameters ranged between 7.22–55.9 N·s/m for b_1 and 2.47–30.56 N·s/m for b_2, which was in the range of 4–175 N·s/m reported by literature.

The variance models identified by the current study were new to literature, so they cannot be directly compared to others. However, they were able to capture all of the experimental variation from the nine subjects and three grip forces. Also, the variance models were computationally-simple, minimum-phase and stable transfer functions that are useful for robust stability analysis and haptic interface design. Specifically, the models introduce experimentally-derived uncertainty bounds for the human operator, which can be used to evaluate the H_∞ robust stability of a haptic interface system as described in [26].

V. CONCLUSION

In conclusion, a unique model structure of the arm and hand dynamics, including the dynamics of the PHANToM haptic interface, was introduced for the human arm using a stylus-based haptic device. The identified parameters were consistent with literature and the models were shown to exhibit frequency responses accurate with respect to the experimental data. Also, the current work introduced a set of experimentally-derived variance models for the X, Y, and Z axes that were new to literature and useful for haptic interface stability analysis and design.

REFERENCES

[1] H. Gomi, Y. Koike, and K. M., "Human hand stiffness during discrete point-to-point multi-joint movement," *Proc. of the Annual International Conference of the IEEE EMBS*, vol. 14, pp. 1628–1629, October - November 1992.

[2] K. J. Kuchenbecker, J. G. Park, and G. Niemeyer, "Characterizing the human wrist for improved haptic interaction," in *Proceedings of the ASME International Mechanical Engineering Congress and Exposition (IMECE 2003)*, vol. 2, 2003, (Paper Number 42017).

[3] L. A. Jones and H. I. W., "Influence of the mechanical properties of a manipulandum on human operator dynamics: elastic stiffness," *Biological Cybernetics*, no. 62, pp. 299–307, 1990.

[4] ——, "Influence of the mechanical properties of a manipulandum on human operator dynamics: viscocity," *Biological Cybernetics*, no. 69, pp. 295–303, 1993.

[5] N. Hogan, "Controlling impedance at the man/machine interface," *Proc. of the IEEE International Conference on Robotics and Automation, Scottsdale, AZ*, vol. 3, pp. 1621–1631, May 1989.

[6] R. J. Adams and B. Hannaford, "A two-port framework for the design of unconditionally stable haptic interfaces," *Proc. of the 1998 IEE/RSJ Int. Conf. on Intelligent Robots and Systems*, pp. 1254–1259, 1998.

[7] J. Winters, L. Stark, and S.-N. A. H., "An analysis of the sources of musculoskeletal system impedance," *Journal of Biomechanics*, vol. 21, no. 12, pp. 1011–1025, 1988.

[8] J. B. MacNeil, R. E. Kearney, and I. W. Hunter, "Time-varying identification of human joint dynamics," *Proc. of the 11th IEEE EMBS Inter. Conf.*, 1989.

[9] C. C. Gielen and J. C. Houk, "Nonlinear viscosity of human wrist," *Journal of Neurophysiology*, vol. 52, no. 3, pp. 553–569, September 1984.

[10] T. Tsuji, K. Goto, M. Moritani, M. Kaneko, and P. Morasso, "Spatial characteristics of human hand impedance in multi-joint arm movements," in *Proceedings of the IEEE International Conference on Intelligent Robots and Systems*, vol. 1, September 1994, pp. 423–430.

[11] R. E. Kearney and I. W. Hunter, "System identification of human joint dynamics," *Critical Reviews in Biomedical Engineering*, vol. 18, no. 1, pp. 55–87, 1990.

[12] D. A. Lawrence, "Stability and transperancy in bilateral teleoperation," *IEEE Transactions on Robotics and Automation*, vol. 9, no. 5, pp. 624–637, October 1993.

[13] K. Kosuge, Y. Fujisawa, and F. T., "Control of mechanical system with man-machine interaction," *Proc. of the IEEE/RSJ International Conference on Intelligent Robots and Systems*, pp. 87–92, 1992.

[14] C. J. Hasser and M. R. Cutkosky, "System identification of the human grasping a haptic knob," *Proc. of the 10th Symposium on Haptic Interfaces for Virtual Environment and Teleoperator Systems, Orlando, FL*, pp. 117–180, March 2002.

[15] H. Woo and D. Lee, "Exploitation of the impedance and characteristics of the human arm in the design of haptic interfaces," *IEEE Transactions on Industrial Electronics*, vol. 56, no. 9, p. in press, 2009.

[16] R. G. Dong, D. E. Wecome, T. W. McDowell, and T. Z. Wu, "Biodynamic response of human fingers in a power grip subjected to a random vibration," *Journal of Biomechanical Engineering*, vol. 126, pp. 447–457, August 2004.

[17] E. Vlugt and A. C. Schouten, "Identification of intrinsic and reflexive muscle parameters of the human arm in 3d joint space," *Proc. of the 2004 IEEE Int. Conf. on Systems, Man, and Cybernetics*, pp. 2471–2478, 2004.

[18] J. E. Speich, L. Shao, and M. Goldfarb, "Modeling the human hand as it interacts with a telemanipulation system," *Mechatronics*, vol. 15, no. 9, pp. 1127–1142, November 2005.

[19] G. Niemeyer and J. J. E. Slotine, "Stable adaptive teleoperation," *IEEE Journal of Oceanic Engineering*, vol. 16, no. 1, pp. 152–162, January 1991.

[20] M. C. Çavuşoğlu, A. Sherman, and F. Tendick, "Design of bilateral teleoperation controllers for haptic exploration and telemanipulation of soft environments," *IEEE Transactions on Robotics and Automation*, vol. 18, no. 4, pp. 641–647, August 2002.

[21] L. Ljung, *System Identification: Theory for the User*, 2nd ed. PTR Prentice-Hall, Upper Saddle River, NJ, 1999.

[22] E. Brenner and J. B. J. Smeets, "Fast responses of the human hand to changes in target position," *Journal of Motor Behavior*, vol. 29, no. 4, pp. 297–321, December 1997.

[23] R. Shadmehr and S. P. Wise, *The Computational Neurobiology of Reaching and Pointing, A Foundation for Motor Learning*, ser. Computational Neuroscience Series, T. J. Sejnowski and T. A. Poggio, Eds. Cambridge, MA: The MIT Press, 2005.

[24] J. E. Marsden and T. J. R. Hughes, *Mathematical foundations of elasticity*. Englewood Cliffs, NJ, USA: Prentice-Hall, Inc., 1983.

[25] M. C. Çavuşoğlu, D. Feygin, and F. Tendick, "A critical study of the mechanical and electrical properties of the PHANToM^{TM} haptic interface and improvements for high performance control," *Presence*, vol. 11, no. 6, pp. 555–568, December 2002.

[26] K. Zhou, J. C. Doyle, and K. Glover, *Robust and Optimal Control*. Edgewood Cliffs, NJ: Prentice Hall, 1996.